Chapter 7

Slow Light in a Silicon-Based Waveguide

7.1 Introduction

Slow light, which means the phenomenon of light propagation in media and structures with a reduced group velocity, has been studied for a long time. It can be traced to the nineteenth century, when the classical theory of dispersion of the electromagnetic waves was first formulated in the works of Lorentz [1]. Slow wave propagation has also been observed and widely used in the microwave range since as early as the 1940s [2, 3].

Going by this history and benefiting from the rapid developments of the technologies required practical implementation of slow light; slow light has become a rapidly growing field with great scientific value and a lot of potential applications. Especially, the recent research on slow light has indicated a variety of potential applications. Examples are given for variable optical delay lines or optical buffers of high-capacity communication networks [4, 5], optical pulse synchronization and reshaping [6], ultrafast all-optical information processing, quantum computing [7], nonlinear optical devices [8], true-time delay in a phased-array antenna [9, 10], optical gyroscope and sensing [11–14], and miniaturization of spectroscopy systems. So far, slow-light propagation has been observed in a

Silicon-Based Photonics
Erich Kasper and Jinzhong Yu

ISBN 978-981-4303-24-8 (Hardcover), 978-1-315-15651-4 (eBook)
www.jennystanford.com

wide variety of media and structures, including Bose–Einstein condensates, low-pressure metal vapors, solid crystal materials, optical fibers, semiconductor quantum wells and quantum dots, and photonic bandgap structures. Silicon-based optical waveguides are important kinds of slow light schemes because silicon is not only a mature semiconductor device and integrated circuit material but also an excellent photonic material. Silicon-based waveguides, especially SOI-based devices, possess the merits of a small footprint and fabrication compatibility with the complementary metal-oxide-semiconductor (CMOS) technology.

Considerable theoretical and experimental attention to realize slow light helped identify the use of silicon-based waveguides, including silicon microring resonators and silicon-based photonic crystals. In this chapter, we will introduce the foundation of slow light in microring resonators and photonic crystal waveguides (PCWs) and present the important experimental progress.

7.2 Concept

The understanding of slow light is based on the concept of group velocity. Let us recall the distinction between the phase velocity and the group velocity of a light wave.

The phase velocity describes the speed at which the phase of the wave propagates. It can be defined as $v_p = \omega/k = c/n$, where ω is the angular frequency of the light and k is the wave number. And the group velocity gives the velocity with which a pulse of light propagates through a material or structure system. It can be defined as $v_g = \partial\omega/\partial k$. Slow light indicates that the group velocity v_g is much less than the velocity c of light in vacuum. Correspondingly, there is also a concept of fast light (superluminal), when $v_g > c$. The speed of a signal cannot be higher than the phase velocity. A negative group velocity corresponds to the case when the group velocity opposes the phase velocity [15].

Note that the refractive index of the medium $n(k, \omega)$ may be described as a function of the frequency ω of the light as well as a function of the propagation constant k because the dispersion relation connects both quantities. According to the definition of the group velocity and the relationship $k = n\omega/c$, one can get

$$\upsilon_{\mathrm{g}} = \frac{c - \omega \dfrac{\partial n(k,\omega)}{\partial k}}{n(k,\omega) + \omega \dfrac{\partial n(k,\omega)}{\partial \omega}} \tag{7.1}$$

From Eq. 7.1, there are two ways to reduce the group velocity v_{g} as follows: (i) make n larger and (ii) make $\partial n/\partial \omega$ positive. An arbitrary combination of either of the above methods can be used to reduce the group velocity.

The first choice is not favored because the limited range of refractive index variations restricts the possible reductions of the group velocity v_{g}. Thus, we focus on the ways of making $\partial n/\partial \omega$ or $\partial n/\partial k$ positive and large to realize slow light. Since the functional dependence $n(\omega)$ originates from the material response and the dependence $n(k)$ is best understood from a nonuniform refractive index distribution, we name $\partial n/\partial \omega$ as material dispersion and $\partial n/\partial k$ as waveguide dispersion (or structure dispersion).

The time for a pulse to pass through the optical medium is known as group delay, which can be generally represented as

$$\tau_{\mathrm{g}} = L / \upsilon_{\mathrm{g}}, \tag{7.2}$$

where L is the physical length of the propagation medium. When the light field experiences a phase shift of $\phi(\omega)$ as it propagates in a medium, the group delay time can also defined as [16]

$$\tau_{\mathrm{g}} = -\frac{\mathrm{d}\varphi(\omega)}{\mathrm{d}\omega} \tag{7.3}$$

7.3 Slow Light in Microring Resonator Waveguides

Microring resonators are important components for modern integrated optics that have numerous applications in communication filters [17, 18], optical modulators and switches [19, 20], optical signal processing [21], laser systems [22, 23], and optical sensing [24]. Besides, studies suggest that microring resonators, together with their cascaded structures, are also an excellent slow light element.

For a single microring, there are two types of configuration: all-pass filter (APF) (Fig. 7.1a) and add-drop (Fig. 7.1b) configuration. There are also two main types of cascaded structures: coupled-resonator optical waveguides (CROWs) [25] and side-coupled integrated sequence of spaced optical resonators (SCISSORs) [26, 27]. A CROW is a chain of resonators in which light propagates by virtue of the direct coupling between the adjacent resonators (Fig. 7.1c). In contrast, a SCISSOR consists of a chain of resonators

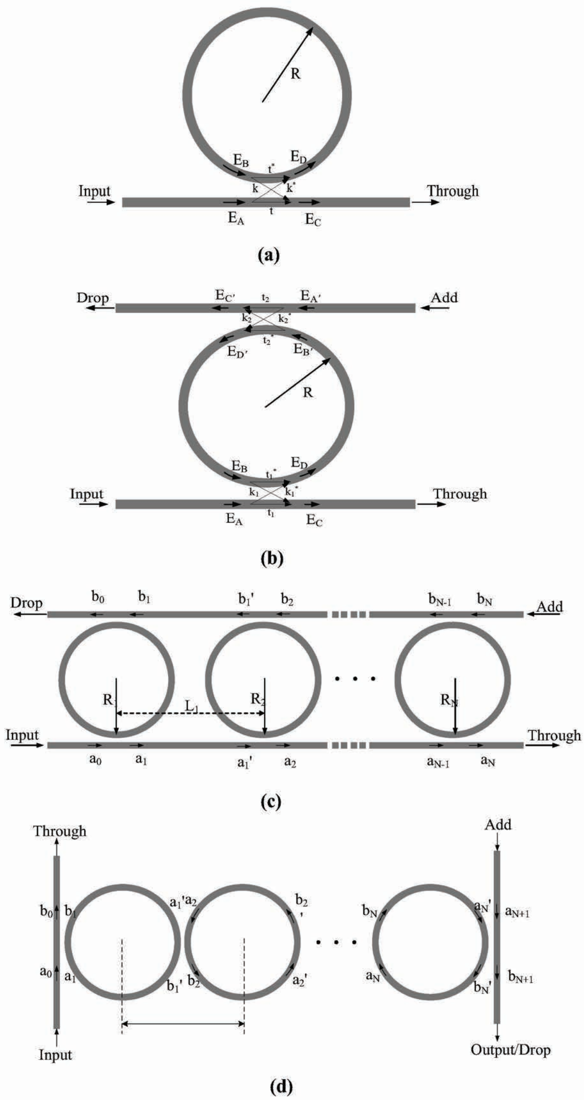

Figure 7.1 The schematic drawing of a single microring and cascaded microrings: (a) all-pass filter (APF) single ring, (b) add-drop single ring, (c) SCISSOR configuration microrings, and (d) CROW configuration microrings.

not directly coupled to each other but coupled through at least one side-coupled waveguide (Fig. 7.1d). Both CROWs and SCISSORs have the potential to significantly slow down the propagation of light. This part deals with slow light in a single-microring resonator as well as the two types of cascaded structured microring resonator waveguides.

7.3.1 Single-Microring Resonator

Figure 7.1 shows the two basic types of single-ring configuration, APF and add-drop single ring. Using transfer matrixes to analyze the characteristic of the add-drop single ring, we can get the properties of the APF single ring by setting the coupling efficient of the add-drop ring to the drop waveguide to zero.

In the schematic of a add-drop single ring, $E_{\mathrm{A}}(E_{\mathrm{A}}^{'}),E_{\mathrm{B}}(E_{\mathrm{B}}^{'}),E_{\mathrm{C}}(E_{\mathrm{C}}^{'}),E_{\mathrm{D}}(E_{\mathrm{D}}^{'})$ represent the local optical fields in the waveguide and the ring of the coupling region, and the field relations can be expressed by a transfer matrix. The coupling coefficient κ and transmission coefficient t satisfy the relation $t_i = \sqrt{1-\kappa_i^2}$ (i = 1, 2). The index i refers to the input line (i = 1) and the drop line (i = 2). We attributed all sources of loss (material absorption, radiation, and scattering) inside the ring to the field transmission γper round in the ring.

The single-pass phase shift is $\varphi(\lambda) = n_{\mathrm{eff}}(\lambda)\cdot\frac{2\pi}{\lambda}\cdot 2\pi R$.

The typical transmission spectra for the trough port (red line) and the drop port (blue line) are plotted in Fig. 7.2.

One can see from the spectra in Fig. 7.2 that when the ring is on-resonance, light is directed to the drop port, and when the ring is off-resonance, light goes to the trough port. When the minimal transmission for the trough port at the resonant wavelength λ_0 equals 0, the ring reaches a critical state that is defined as critical coupling. It means that the coupling between the input waveguide and the ring is equal to the loss per round in the ring times the coupling between the output (drop) waveguide and the ring. This state requires that

$$t_1 = t_2 \cdot e^{-\gamma} \tag{7.4}$$

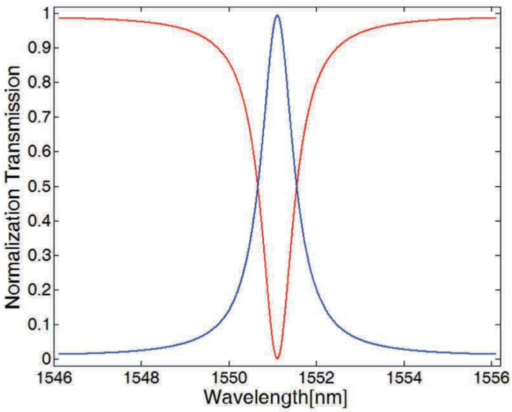

Figure 7.2 Typical transmission spectra of the trough port (red line) and the drop port (blue line) for the microring resonator in the add-drop configuration.

Similarly, $t_1 > t_2 \cdot e^{-\gamma}$ represents the undercoupling state and $t_1 < t_2 \cdot e^{-\gamma}$ represents the overcoupling state, which means the coupling t_1 between the input waveguide and the ring is more or less than the loss $\exp(-\gamma)$ per round in the ring times the coupling t_2 between the output waveguide and the ring, respectively. The coupling state is closely related to the slow light condition, which will be discussed later.

From the transfer matrix, we can also get the effective phase shift at both the trough and the drop port and the group delay time according to the definition Eq. 7.3.

We can get the transfer characteristic, phase shift characteristic, as well as delay characteristic of an APF single ring when the coupling efficiency of the add-drop ring to the drop waveguide is zero.

Let us now discuss the relationship between the coupling and delay characteristics of a single ring. The delay time is a periodic function of wavelength for a fixed coupling states (over- or undercoupling state), which exhibits sharp peaks at $\phi = 2N\pi$. The delay time at $\cos\phi = 1$ is

$$\tau_\mathrm{d}\,|_{\lambda_0} = -\frac{(1-t^2)\cdot e^{-\gamma}}{(e^{-\gamma}-t)(1-t\cdot e^{-\gamma})}\cdot\frac{n_\mathrm{g}\cdot 2\pi R}{c}. \tag{7.5}$$

At the critical coupling point of the APF single ring, that is, $e^{-\gamma} = t$, the denominator of Eq. 7.5 equals zero. As a result Eq. 7.5 displays a very violent behavior in this region associated with the fact that the effective phase shift changes sign near resonance as coupling crosses the critical point. For $e^{-\gamma} > t$, the ring is overcoupled and the group delay time τ_d has a positive value at resonance, indicating that the light pulse is trapped and spends a relatively long time circulating in the ring and so the ring exhibits a slow light mode. On decreasing $e^{-\gamma}$ while keeping t fixed, τ_d becomes a large positive value as $e^{-\gamma}$ approaches its critical value, then flips to a large negative value as $e^{-\gamma}$ enters the $e^{-\gamma} < t$ region and finally decreases in magnitude (remaining negative) as $e^{-\gamma}$ is further decreased. Figure 7.3 shows the group delay time as a function of wavelength for an APF single ring in different coupling states, in which $t = 0.97$ is kept fixed.

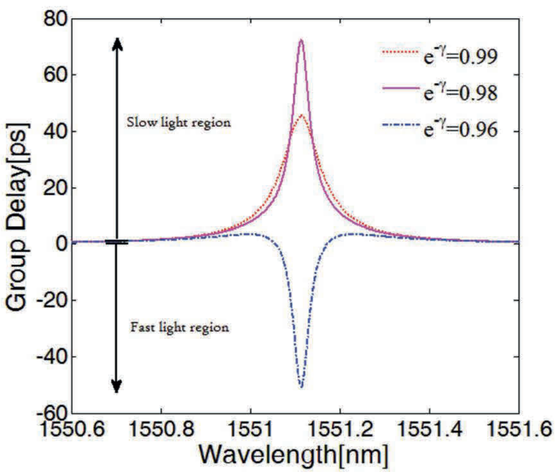

Figure 7.3 Group delay time as a function of wavelength for an APF single ring with a fixed $t = 0.97$.

7.3.2 SCISSOR Configuration Microring Resonators

On the basis of the transfer matrix analysis of a single ring, we can also get the dispersion relation of a SCISSOR. The local optical fields of the SCISSOR are labeled in Fig. 7.1c.

To find the modes and dispersion relation of a SCISSOR configuration, applying the Bloch boundary conditions, we get

$$\begin{bmatrix} a_1' \\ b_1' \end{bmatrix} = \exp(jK\Lambda)\begin{bmatrix} a_0 \\ b_0 \end{bmatrix}, \tag{7.6}$$

where K is the Bloch wave number and $\Lambda = L_1$ is the Bragg period. This relation strictly applies only for an infinite periodic array, but we will see that the photonic band structure exists even for a finite array.

A typical dispersion relation of a SCISSOR structured microring is depicted in Fig. 7.4, from which, one can see that the dispersion relation consists of passbands and bandgaps. Furthermore, the dispersion relation exhibits two types of bandgaps [28]: one is direct gap, which means that there is no discontinuity in the Bloch wave vector between the lower and upper band edge frequencies, and the other is indirect gap, where the wave vectors between the upper and lower band edge frequencies differ by π/Λ. The two types of bandgaps stem from the Bragg reflection and the resonant reflection in SCISSOR structures; thus they are called the "resonant gap" and the "Bragg gap," respectively. If the frequency of the light is close to the Bragg frequency, the additional phase shift induced by successive unit cells of the system is an integer multiple of 2π, and a weak coupling can be enhanced via a Bragg-type process of constructive interference of reflections. Therefore, a Bragg gap arises in the dispersion relation.

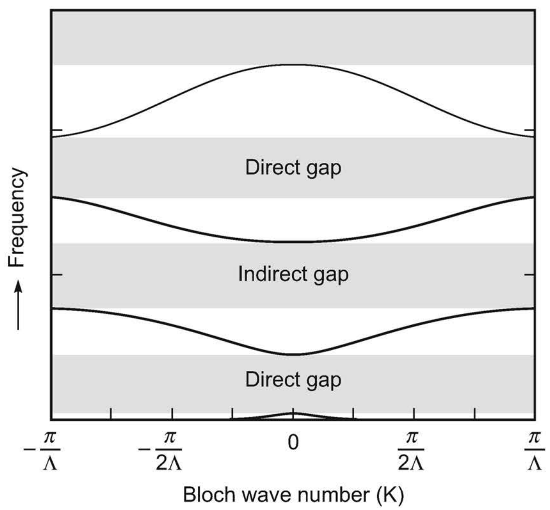

Figure 7.4 Typical SCISSOR dispersion relation.

For a frequency close to the resonance frequency of the resonator, the effective coupling between the two channels can become quite large and a gap also arises. This gap is the called the "resonator gap." Near the band edge frequencies, the dispersion relation is flat and the group velocity approaches zero and this is a slow light regime.

7.3.3 CROW Configuration Microring Resonators

There are three methods to analyze the CROW configuration microring: tight-binding formalism [25], transfer matrixes [29], and temporal coupled-mode theory [30]. The three methods of analysis produce an identical form of the dispersion relation in the limit of weak coupling [31]. Here we chose to revisit the matrix analysis above.

In the tight-binding method, we approximate the electric field of an eigenmode $\vec{E}_{\mathrm{k}}$ of the CROW as a Bloch wave superposition of the individual resonator modes.

Substituting the Bloch waves into Maxwell's equations and taking the assumption of symmetric nearest-neighbor coupling, after some algebra, we find that the dispersion relation of the CROW is:

$$\omega_K = \omega_0[1 - \frac{\Delta\alpha}{2} + \kappa\cos(K\Lambda)] \tag{7.7}$$

Here ω_K is the frequency of the eigenmode in the CROW chain, ω_0 is the resonance frequency of an individual resonator, the coupling parameter κ represents the overlap of the modes of two neighboring resonators, and $\Delta\alpha$ gives the fractional self-frequency shift centered at ω_0.

A dispersion diagram of a CROW-structured microring is shown in Fig. 7.5a [32]. From the dispersion curve, one can see that the propagation waves in CROW are arranged in narrow bands centered at the resonance frequencies, while at the nonresonance frequencies, the optical wave decays in the CROW and forms the bandgaps. The group velocity in a CROW, which corresponds to the slope of the dispersion curve, is given by

$$\upsilon_{\mathrm{g}} = \frac{\mathrm{d}\omega_K}{\mathrm{d}K} = -\omega_0\Lambda\kappa\sin(K\Lambda). \tag{7.8}$$

From this formula of v_{g} and the dispersion curve, it can be seen that the group velocity is maximum at the center of the passband, where $\sin(K\Lambda) = 1$, and zero at the band edges, where $\sin(K\Lambda) = 0$. Besides, we can see that the group velocity depends on the coupling efficient κ between the microrings and on the periodicity of the CROW.

To achieve slow-light propagation, the coupling between the microrings must be weak to attain a relatively flat propagation band in the dispersion relation. A small value of group velocity can be acquired for a weakly coupled CROW or compact CROW. Figure 7.5b shows the normalized group velocity as a function of the normalized frequency, which gives a visualization of the characteristics.

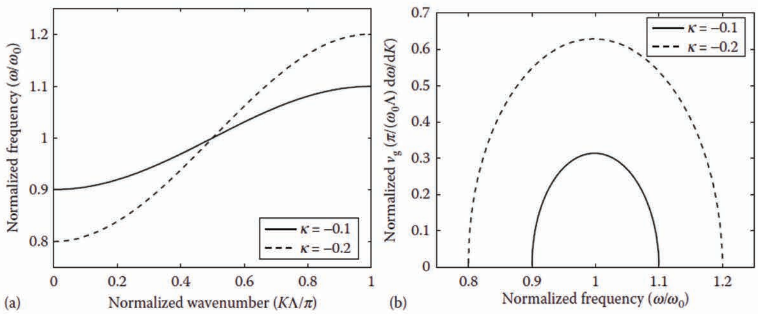

Figure 7.5 (a) Dispersion diagram and (b) the normalized group velocity of a CROW for various values of κ and $\Delta\alpha$ = 0. Copyright (2008) From Ref. [32]. Reproduced by permission of Taylor and Francis Group, LLC, a division of Informa plc.

7.3.4 Experimental Progress

With the improvement of microelectronic fabrication and high-index-contrast silicon waveguide technology, ultracompact and large-scale cascaded microrings for slow light have been demonstrated. Besides, to get tunable group delays, some tuning mechanisms, like the thermo-optic effect, were introduced to change the refractive index of the waveguides.

On the basis of the SOI photonic wire waveguides, a research group of IBM realized 56-microring resonators cascaded in SCISSOR configuration and 100 microring resonators cascaded in CROW configuration to achieve a large group delay [33]. The SEM pictures of the optical delay lines are shown in Fig. 7.6. An on-resonance group delay of 510 ps is observed in the time-domain measurements of a 1 Gbps pseudorandom bit stream of optical pulses in a non-return-to-zero format, transmitted through the 56-microring SCISSOR, and the value is 220 ps for the 100-microring CROW.

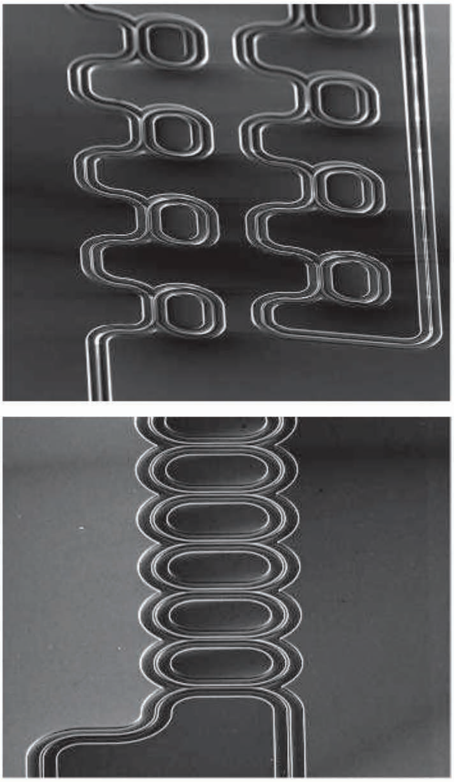

Figure 7.6 Scanning electron micrographs of resonantly enhanced optical delay lines based on photonic-wire waveguides. Reprinted by permission from Springer Nature Customer Service Centre GmbH: Springer Nature, *Nature Photonics*, Ref. [33], copyright (2006).

A balanced SCISSOR delay structure, which allows for an increased bandwidth and continuous tunability of group delay, was demonstrated [34]. In the balanced SCISSOR, the resonant frequencies of the rings are shifted by a small amount $\Delta\omega$ from a center resonant frequency ω_r. Half of the rings are blue-shifted, and the other half are red-shifted compared to the center frequency. This arrangement cancels the third-order group delay dispersion. Even though the resonances of the rings are changed about the central resonant frequency ω_r, the operating frequency of the overall structure remains the same while the group delay significantly changes. The spectral width of the structure, therefore, broadens, increasing its bandwidth. Using standard CMOS fabrication processes, the device consisted of eight SOI-based microrings with Cr heaters. The measurement of the device shows a continuously tunable delay of up to 72 ps operating on 100 ps pulses without introducing distortion, which can be used as on-chip buffers in optical interconnects and signal processing applications.

7.4 Slow Light in Photonic Crystals

PCWs are known for providing large group index dispersion together with very low values of group velocity. A "group velocity refractive index," usually called the "group index" is defined as the ratio of light velocity c to group velocity v_g. This value should not be confused with the refractive index n, which is always defined with respect to the phase velocity.

Slow-light propagation in PCWs is a hot research topic, and group velocities below $c/300$ were early demonstrated [35]. Like slow light in microring resonators, slow light in PCWs is controlled by dispersion from waveguide structures. PCWs offer more bandwidth than any other schemes in a slow light regime. However, loss issues may be one of the challenges for PCW slow light applications.

7.4.1 Generation of Slow Light in a Photonic Crystal Waveguide

A photonic crystal is primarily a grating, and most of the slow light effects can be explained from a 1D grating perspective. In fact, the coupled resonator structures discussed in the preceding section fall into the same category. Photonic crystals are conveniently described by their band structure, which is described as an energy wave vector ($\omega - k$) diagram of the allowed states or modes of the crystal.

The simplest dispersion curve is shown in Fig. 7.7a, which describes a wave propagating in a dispersion-free medium, namely a straight line with a constant slope. In fact, the constant slope denotes the phase velocity, which is defined as $v_p = \omega/k$. For free space, we have $v_p = c = \omega/k$; for a material of refractive index n, $v_p = c/n = \omega/k$. In a periodically structured medium such as a 1D grating, the dispersion curve is no longer a straight line but now features a discontinuity; see Fig. 7.7b. The discontinuity breaks the dispersion curve into multiple bands consisting of some passbands spaced with stop-bands, namely the PBG features. Only light at the frequency in the passbands can be guided in the structure, while light of the frequency in the stop-band is reflected. In proximity of this stop-band, the dispersion curve is no longer a straight line and one needs to distinguish between the phase velocity and the group velocity $v_g = \partial\omega/\partial k$, the latter denoting the local slope of the curve. From Fig. 7.7b, at the edge of the stop-band, the slope of the dispersion curve is flat, indicating that the group velocity is zero. On the other hand, near the stop-band, the local slope of the curve, namely the group velocity, is larger than zero but much smaller than the phase velocity.

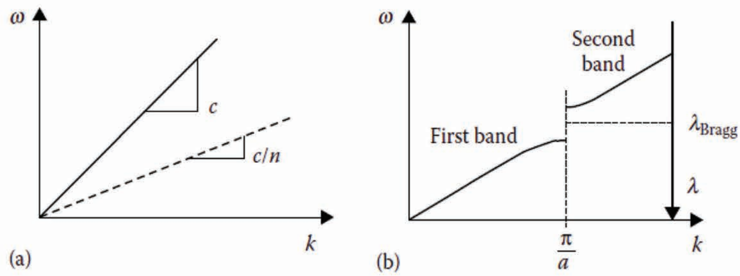

Figure 7.7 Dispersion diagram for (a) an optical wave propagating in free space (solid line) and a medium with a constant refractive index n (dashed line) and (b) an optical wave propagating in a periodic medium. Copyright (2008) From Ref. [32]. Reproduced by permission of Taylor and Francis Group, LLC, a division of Informa plc.

What's the nature of slow light in PCWs? There are two possible mechanisms, backscattering and omnidirectional reflection, to illustrate slow-light propagation in PCWs [36], invoking the familiar ray picture commonly used to describe light propagation in a dielectric waveguide. For backscattering, light is coherently backscattered at each unit cell of the photonic crystal, so the photonic crystal acts as a 1D grating (indicated by the vertical lines on the left in Fig. 7.8). At the Brillouin zone boundary for $k = 0.5 \times 2\pi/a$, the forward propagating and the backscattered light agree in phase and amplitude and a standing wave results, which can also be understood as a slow mode with zero group velocity. If the incident light frequency moves away from the Brillouin zone boundary, it will fall into the slow light regime and the forward and backward traveling components begin to move out of phase but still interact, resulting in a slowly moving interference pattern—the slow mode.

Further from the Brillouin zone boundary, the forward and backward traveling waves are too out of phase to experience much interaction and the mode behaves like a regular waveguide mode that is dominated by total internal reflection. In Fig. 7.8, the arrows pointing right and left represent the forward and backward traveling components, respectively. The right-pointed arrows are longer, as if the mode was taking three steps forward and two steps back—a slow forward movement. Since the existence of the photonic bandgap, light of proper energy that propagates at any angle is reflected. Even light propagating at or near normal incidence may, therefore, form a mode, as indicated by the steep zig-zag on the right in Fig. 7.8. In band structure terms, this corresponds to propagation along the waveguide at or near the Γ point, that is, $k \approx 0$. It is obvious that such

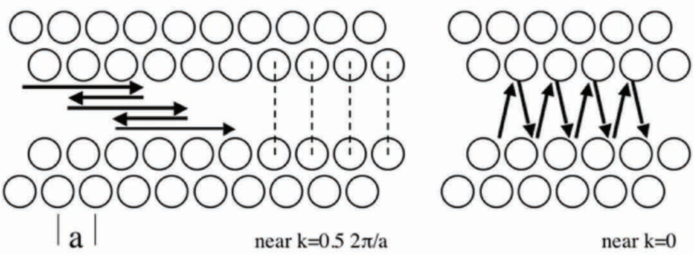

Figure 7.8 Illustration of the two possible mechanisms for achieving slow light in photonic crystal waveguides, namely coherent backscattering (left) and omnidirectional reflection (right). Republished with permission of IOP Publishing, Ltd, from Ref. [36], copyright (2007); permission conveyed through Copyright Clearance Center, Inc.

modes have very small forward components, that is, they travel as slow modes along the waveguide or form a standing wave for $k = 0$.

7.4.2 Experimental Verification of Slow Light in Photonic Crystals

There has been a lot of research work about slow light in PCWs in the last decades, and the covered topics include theoretical exposition [37], experimental observation [38, 39], slow light–enhanced nonlinear effects [40–43], dispersion engineering [44–46], and coupled-nanocavity-enhanced photonic crystals waveguides [47, 48]. Here we review some of the representative works obtained in the early pioneering phase.

Early in 2005, Vlasov et al. had experimentally demonstrated an over 300-fold reduction in the group velocity on a silicon chip via an ultracompact photonic integrated circuit using low-loss silicon PCWs [35]. Figure 7.9 shows the SEM images of the silicon PCWs device they used. To measure the group velocity, an integrated unbalanced Mach–Zehnder interferometer (MZI) structure was designed (Fig. 7.9a). The unbalanced MZI is formed by introducing a small but noticeable difference in the hole radii of the two PCW arms—the signal arm and the reference arm.

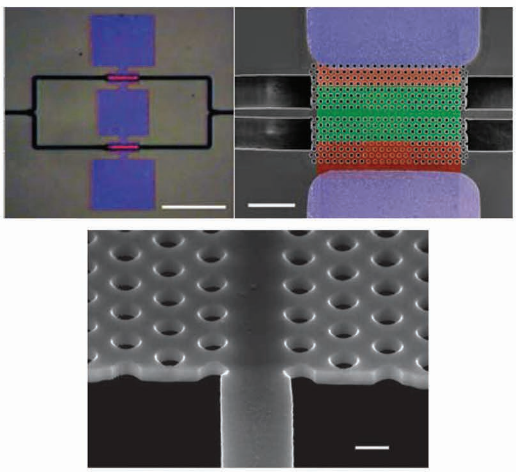

Figure 7.9 SEM images of an active unbalanced Mach–Zehnder interferometer using photonic crystal waveguides. Reprinted by permission from Springer Nature Customer Service Centre GmbH: Springer Nature, *Nature*, Ref. [35], copyright (2005).

Due to the interference between the signal light and the reference light, the frequency becomes nearly independent from the wave number near the bandgap. Very large group indices of up to 500 were found from the transmission spectrum. In addition, optimized ohmic lateral electrical contacts for locally heating the signal arm were fabricated to dynamically tune the dispersion characteristics, thus obtaining active control of slow light. Figure 7.9b shows the definition of the metallic contacts on top of the PCW. Measure of the active MZI device indicates that tunable group indices can be achieved by applying electric power to the signal arm.

Slow light–enhanced nonlinear optical effects have been noticed and utilized. An outstanding representative work is green light emission in silicon through slow-light-enhanced third-harmonic generation (THG) in PCWs [49].

A 2D silicon PCW (see Fig. 7.10) is engineered to display both low group velocity and low dispersion, and the latter feature promises benefits of slow light for nonlinear applications. The measured group velocity of the fundamental mode varies almost linearly by a factor of 4 from $c/10$ to $c/40$ in the spectral window from 1550 to 1559 nm. When a near-infrared 4.5-ps pulse train was launched into the PCW, green light emitting from the surface of the chip was observed by the naked eye (Fig. 7.10). It is illustrated that the green light emission

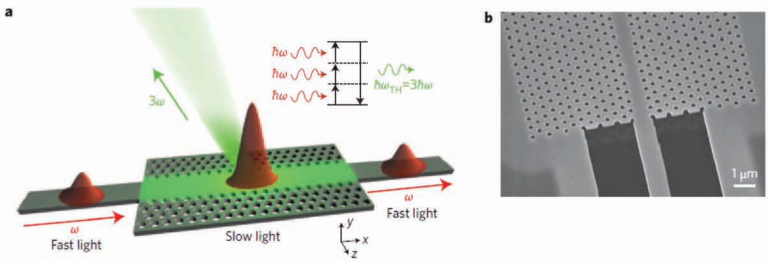

Figure 7.10 Green light emission through third-harmonic generation (THG) in a slow-light photonic crystal waveguide. (a) Schematics of slow light–enhanced THG. The fundamental pulse at a frequency ω is spatially compressed in the slow-light photonic crystal waveguide, increasing the electric field intensity, while the third-harmonic signal, at a frequency $\omega_{TH} = 3\omega$, is extracted out-of-plane by the photonic crystal with a specific angle off the vertical direction. (b) Scanning electron microscopy (SEM) image of the tapered ridge waveguide connected to the photonic crystal waveguide etched in a thin silicon membrane. Scale bar, 1 mm. Reprinted by permission from Springer Nature Customer Service Centre GmbH: Springer Nature, *Nature Photonics*, Ref. [49], copyright (2009).

for only 10 W peak pump powers is due to both the tight light confinement within the PCW and the energy density enhancement provided by the slow light mode. This THG observation further highlights that slow light is favorably utilized to implement the desired functionalities.

7.5 Conclusion

Microring resonators, especially cascaded microring resonators, and photonic crystals are two promising approaches for generating slow light. Progress on both types of structures runs almost in parallel, and the two are competing to become the preferred scheme. Both types of schemes possess potential as well as limits in future application, and each has its own most suitable area of exploitation.

Slow light devices should be evaluated by considering a variety of figures of merit, such as tunability, losses, preservation of the signal quality, reliability, and technology requirements, in addition to the possibility of dynamically controlling the slowdown factor on chip [50].

In recent years, using nonlinear optical effects in hybrid-on silicon emerged as an interesting topic for on-chip all-optical data treatment. Because of their low refractive indexes, the new nonlinear optical materials developed in soft matter science (e.g., polymers and liquids) are delicate for using. However, such materials for using can be incorporated in slot PCWs and hence can benefit from both slow light field enhancement effect and slot-induced ultrasmall effective areas. Reported results [51] provide experimental evidence for accurate control of the dispersion properties of fillable periodical slotted structures [52] in silicon photonics. PCWs appear as good candidates due to their confinement and versatile dispersion properties, including slow light and possible control of group velocity dispersion. Slow light structures [53] show enhancement of the nonlinearity that depends on the group index. Third-order nonlinear effects, such as Kerr self-phase modulation scale, increase with the square of the group index.

Acknowledgments

We thank Yingtao Hu and Yuntao Li for the collection of basic information and figure drawings.

References

1. H. Lorentz (1880). Relation between propagation of light and density of matter, *Wied. Ann. Phys. Chem.*, **9**(4), 641–665.

2. J. R. Pierce (1950). Traveling-wave tubes, *Bell Syst. Tech. J.*, **29**(4), 608–671.
3. L. Field (1949). Some slow-wave structures for traveling-wave tubes, *Proc. IRE*, **37**(1), 34–40.
4. R. W. Boyd (2005). Applications of slow-light in telecommunications and optical switching, Presented at Photonics West.
5. E. Parra and J. Lowell (2007). Toward applications of slow light technology, *Optics and Photonics News*, **18**(11), 40–45.
6. M. Fisher and S. Chuang (2005). Variable group delay and pulse reshaping of high bandwidth optical signals, *IEEE J. Quantum Electron.*, **41**(6), 885–894.
7. M. Fleischhauer and M. Lukin (2002). Quantum memory for photons: dark-state polaritons, *Phys. Rev. A*, **65**(2), 22314.
8. S. Harris and L. Hau (1999). Nonlinear optics at low light levels, *Phys. Rev. Lett.*, **82**(23), 4611–4614.
9. W. Jemison, T. Yost and P. Herczfeld (1996). Acoustooptically controlled true time delays: experimental results, *IEEE Microwave Guided Wave Lett.*, **6**(8).
10. Z. Liu, et al. (2006). X-band continuously variable true-time delay lines using air-guiding photonic bandgap fibers and a broadband light source, *Opt. Lett.*, **31**(18), 2789–2794.
11. F. Zimmer and M. Fleischhauer (2004). Sagnac interferometry based on ultraslow polaritons in cold atomic vapors, *Phys. Rev. Lett.*, **92**(25), 253204.
12. Z. Shi, et al. (2007). Slow-light Fourier transform interferometer, *Phys. Rev. Lett.*, **99**(24), 240804.
13. G. Purves, C. Adams and I. Hughes (2006). Sagnac interferometry in a slow-light medium, *Phys. Rev. A*, **74**(2), 23805.
14. G. Jundt, et al. (2003). Non-linear Sagnac interferometry for pump-probe dispersion spectroscopy, *Eur. Phys. J. D*, **27**(3), 273–276.
15. C. Garrett and D. McCumber (1970). Propagation of a Gaussian light pulse through an anomalous dispersion medium, *Phys. Rev. A*, **1**(2), 305–313.
16. G. Lenz, B. J. Eggleton, C. K. Madsen and R. E. Slusher (2001). Optical delay lines based on optical filters. *IEEE J. Quantum Electron.*, **37**, 525–532.
17. C. Madsen and J. Zhao (1999). *Optical Filter Design and Analysis: A Signal Processing Approach* (John Wiley & Sons, Inc. New York, NY, USA).

18. C. Madsen (2000). General IIR optical filter design for WDM applications using all-pass filters, *J. Lightwave Technol.*, **18**(6), 860.
19. Q. Xu, et al. (2007). 12.5 Gbit/s carrier-injection-based silicon micro-ring silicon modulators, *Opt. Express*, **15**(2), 430–436.
20. S. Emelett and R. Soref (2005). Design and simulation of silicon microring optical routing switches, *J. Lightwave Technol.*, **23**(4), 1800.
21. V. Van, et al. (2002). Optical signal processing using nonlinear semiconductor microring resonators, *IEEE J. Sel. Top. Quantum Electron.*, **8**(3), 705–713.
22. B. Liu, A. Shakouri and J. Bowers (2004). Passive microring-resonator-coupled lasers, *Appl. Phys. Lett.*, **79**, 3564.
23. Z. Bian, B. Liu and A. Shakouri (2003). InP-based passive ring-resonator-coupled lasers, *IEEE J. Quantum Electron.*, **39**(7), 859–865.
24. A. Yalcin, et al. (2006). Optical sensing of biomolecules using microring resonators. *IEEE J. Sel. Top. Quantum Electron.*, **12**(1), 148–155.
25. A. Yariv, et al. (1999). Coupled-resonator optical waveguide: a proposal and analysis, *Opt. Lett.*, **24**(11), 711–713.
26. J. Heebner and R. Boyd (2002). Slow' and fast 'light in resonator-coupled waveguides, *J. Mod. Opt.*, **49**(14/15), 2629–2636.
27. J. Heebner, R. Boyd and Q. Park (2002). SCISSOR solitons and other novel propagation effects in microresonator-modified waveguides, *J. Opt. Soc. Am. B*, **19**, 722–734.
28. J. Heebner (2003). Nonlinear optical whispering gallery microresonators for photonics, PhD thesis, University of Rochester.
29. J. Poon et al. (2004). Matrix analysis of microring coupled-resonator optical waveguides, *Opt. Express*, **12**(1), 90–103.
30. J. Poon and A. Yariv (2007). Active coupled-resonator optical waveguides. I. Gain enhancement and noise, *J. Opt. Soc. Am. B*, **24**(9), 2378–2388.
31. J. Poon, et al. (2004). Designing coupled-resonator optical waveguide delay lines, *J. Opt. Soc. Am. B*, **21**(9), 1665–1673.
32. J. Khurgin (2008). *Slow Light: Science and Applications* (CRC Press).
33. F. Xia, L. Sekaric and Y. Vlasov (2007). Ultracompact optical buffers on a silicon chip, *Nat. Photonics*, **1**(1), 65–74.
34. J. Cardenas, et al. (2009). Large bandwidth continuously tunable delay using silicon microring resonators, in *Group IV Photonics 2009*.
35. Y. Vlasov, et al. (2005). Active control of slow light on a chip with photonic crystal waveguides, *Nature*, **438**(7064), 65–69.

36. T. Krauss (2007). Slow light in photonic crystal waveguides, *J. Phys. D: Appl. Phys.*, **40**, 2666–2670.
37. S. Zhu, et al. (2000). Time delay of light propagation through defect modes of one-dimensional photonic band-gap structures, *Opt. Commun.*, **174**(1–4), 139–144.
38. H. Gersen, et al. (2005). Real-space observation of ultraslow light in photonic crystal waveguides, *Phys. Rev. Lett.*, **94**(7), 73903.
39. T. Kawasaki, D. Mori and T. Baba (2007). Experimental observation of slow light in photonic crystal coupled waveguides, *Opt. Express*, **15**(16), 10274–10284.
40. M. Soljačić, et al. (2002). Photonic-crystal slow-light enhancement of nonlinear phase sensitivity, *J. Opt. Soc. Am. B*, **19**(9), 2052–2059.
41. B. Corcoran, et al. (2009). Optical performance monitoring via slow light enhanced third harmonic generation in silicon photonic crystal waveguides, *Conference on Optical Fiber Communication*, San Diego, CA, USA.
42. Y. Hamachi, S. Kubo and T. Baba (2009). Slow light with low dispersion and nonlinear enhancement in a lattice-shifted photonic crystal waveguide, *Opt. Lett.*, **34**(7), 1072–1074.
43. K. Inoue, et al. (2009). Enhanced third-order nonlinear effects in slow-light photonic-crystal slab waveguides of line-defect, *Opt. Express*, **17**(9), 7206–7216.
44. S. Ha, et al. (2008). Dispersionless tunneling of slow light in antisymmetric photonic crystal couplers, *Opt. Express*, **16**(2), 1104–1114.
45. T. Baba, et al. (2009). Dispersion-controlled slow light in photonic crystal waveguides, *Proc. Jpn. Acad. Ser. B: Phys. Biol. Sci.*, **85**(10), 443–453.
46. M. Ebnali-Heidari, et al. (2009). Dispersion engineering of slow light photonic crystal waveguides using microfluidic infiltration, *Opt. Express*, **17**(3), 1628–1635.
47. M. Notomi, E. Kuramochi and T. Tanabe (2008). Large-scale arrays of ultrahigh-Q coupled nanocavities, *Nat. Photonics*, **2**(12), 741–747.
48. M. Svaluto Moreolo, V. Morra and G. Cincotti (2008). Design of photonic crystal delay lines based on enhanced coupled-cavity waveguides, *J. Opt. A: Pure Appl. Opt.*, **10**, 064002.
49. B. Corcoran, et al. (2009). Green light emission in silicon through slow-light enhanced third-harmonic generation in photonic-crystal waveguides, *Nat. Photonics*, **3**(4), 206–210.

50. A. Melloni, F. Morichetti and T. Krauss (2009). Slow light in coupled ring resonators and PhC: a comparison, *Advances in Optical Sciences Congress*, OSA Technical Digest (CD) (Optical Society of America, 2009), paper STuC3.

51. S. Serna, P. Colman, W. Zhang, X. Le Roux, C. Caer, L. Vivien and E. Cassan (2016). Experimental GVD engineering in slow light slot photonic waveguides, *Sci. Rep.*, **6**, 26956.

52. J. Leuthold, C. Koos and W. Freude (2010). Nonlinear silicon photonics, *Nat. Photonics*, **4**, 535–544.

53. L. Vivien and L. Pavesi (2013). *Handbook of Silicon Photonics* (CRC Press).